Research Square

Preprints are preliminary reports that have not undergone peer review.
They should not be considered conclusive, used to inform clinical practice,
or referenced by the media as validated information.

Power Quality Enhancement in Industrial Networks Using a Transformerless Shunt Hybrid Active Power Filter with MVF-PLL: System Design and Experimental Validation

Mustapha SARRA

mustapha.sarra@univ-bba.dz

University Mohamed El Bachir El Ibrahimi of Bordj Bou Arreridj

Research Article

Keywords: Converter control, Harmonics mitigation, Multi-Variable Filter (MVF), Phase-Locked Loop (PLL), Power quality improvement, Shunt Hybrid Active Power Filter (SHAPF), Voltage Source Inverter (VSI)

Posted Date: October 30th, 2026

DOI: https://doi.org/10.21203/rs.3.rs-11516612/v1

License: This work is licensed under a Creative Commons Attribution 4.0 International License.
Read Full License

Additional Declarations: No competing interests reported.

Power Quality Enhancement in Industrial Networks Using a Transformerless Shunt Hybrid Active Power Filter with MVF-PLL: System Design and Experimental Validation

Mustapha SARRA[1]

[1]Department of Electronics, Institute of Electronics and Telecomunications, University of Bordj Bou Arreridj, El Anasser, Bordj Bou Arreridj, Algeria.

[1]E.T.A Laboratory, University of Bordj Bou Arreridj, El Anasser, Bordj Bou Arreridj, Algeria

*Corresponding author: Mustapha SARRA; mustapha.sarra@ univ-bba.dz

Abstract- This paper proposes a transformerless Shunt Hybrid Active Power Filter (SHAPF) designed to mitigate harmonic distortion and compensate for reactive power demand induced by non-linear industrial loads. The active filter control algorithm is implemented within the Synchronous Reference Frame (SRF) framework, employing a Multi-Variable Filter (MVF) coupled with a robust Phase-Locked Loop (PLL) for precise reference current generation. The structural arrangement comprises a single 7th-harmonic tuned LC passive filter per phase directly interfaced in series with a low-power three-phase Voltage Source Inverter (VSI), eliminating the requirement for a heavy coupling transformer. Consequently, the power rating requirement of the active converter is significantly reduced compared to standard active topologies. The dynamic performance of the system and control algorithm is verified through MATLAB/Simulink modeling and validated on a 20 kVA experimental laboratory setup developed at the LIAS Laboratory, University of Poitiers. Steady-state and dynamic transient results confirm that the proposed SHAPF reduces grid current Total Harmonic Distortion (THD) from 27.38%

down to 2.71% in simulation and 3.9% experimentally, fully meeting IEEE-519 standards.

Keywords- Converter control, Harmonics mitigation, Multi-Variable Filter (MVF), Phase-Locked Loop (PLL), Power quality improvement, Shunt Hybrid Active Power Filter (SHAPF), Voltage Source Inverter (VSI).

1. Introduction

In modern power distribution infrastructures, the continuous deployment of non-linear power electronic loads—such as diode or thyristor rectifiers, adjustable speed drives (ASDs), switch-mode power supplies (SMPS), computer equipment, television sets, telecommunication power units, and industrial electric arc furnaces—has introduced severe power quality challenges in both distributed generation and industrial networks. These non-linear loads draw distorted, non-sinusoidal currents from the AC grid, leading to excessive neutral current flow, heavy reactive power consumption, poor power factor, and voltage distortion at the Point of Common Coupling (PCC). Such power quality degradation compromises overall energy efficiency, causes overheating in distribution transformers, accelerates dielectric insulation aging, and induces severe electromagnetic interference in nearby communication networks.

Historically, Passive Power Filters (PPFs) based on tuned LC networks were widely deployed to suppress harmonic currents and improve power factor due to their structural simplicity and low initial capital investment. Nevertheless, conventional PPFs possess well-documented inherent limitations:

- The requirement to install an independent passive branch for every targeted harmonic order.
- High sensitivity to utility grid frequency variations.

- Vulnerability to component parameter drift over time.
- Rigid tuning frequencies that cannot adapt dynamically.
- The severe risk of parallel or series harmonic resonance with the utility grid impedance.
- To overcome the operational drawbacks of passive filtering, pure Active Power Filters (APFs) based on pulse-width modulated (PWM) Voltage Source Inverters (VSIs) have been extensively researched and commercialized. APFs offer dynamic, continuous, and wideband harmonic attenuation without resonance hazards. However, pure APFs require full-rated power converters scaled for the maximum grid voltage and load current, leading to elevated installation costs, higher switching losses, and financial barriers to widespread industrial implementation. [1-7].

To bridge the gap between low-cost PPFs and high-performance pure APFs, Shunt Hybrid Active Power Filter (SHAPF) topologies have emerged as a cost-effective alternative. By strategically combining a passive filter with a small-rated APF, hybrid configurations inherit the high filtering performance of active topologies while significantly reducing the required power rating and capital cost of the active converter.

This paper describes a transformerless SHAPF system targeted at real-time power quality enhancement in three-phase distribution networks. The proposed configuration directly connects a three-phase VSI in series with a single 7th-harmonic tuned LC passive filter per phase, thereby dispensing with the conventional bulky matching transformer. Designing the passive branch tuned specifically to the 7th harmonic (instead of the typical 5th harmonic) provides key operational benefits:

- It allows the use of smaller, cost-effective inductors (L_F).

- It yields a lower impedance path for higher-order harmonic components such as the 11th and 13th orders.

Grid synchronization is achieved through a robust Phase-Locked Loop (PLL) based on a Multi-Variable Filter (MVF) operating in the stationary $\alpha\beta$ reference frame. The MVF isolates the fundamental frequency voltage component without introducing phase delay or magnitude attenuation. [8]-[11].

2. SHAPF System Architecture and Fundamental Operating Principles

The power schematic of the proposed transformerless SHAPF system designed to maintain the grid current Total Harmonic Distortion (THD_i) below 5% is illustrated in Figure 1. The system is connected to a three-phase, three-wire AC power network supplying a non-linear load represented by a six-pulse diode bridge rectifier feeding an inductive RL load. The active filter stage is directly interfaced with the system through a single LC passive filter per phase, tuned to the 7th harmonic frequency.

In this work, the passive filter branch is intentionally tuned to the 7th harmonic component (350 Hz) rather than the conventional 5th harmonic (250 Hz) for the following technical reasons:

1. **Compact Physical Size:** For an identical inductance value L_F, a passive filter tuned to the 7th harmonic requires smaller, lighter, and less expensive capacitive and inductive components compared to a 5th-harmonic filter.
2. **Superior High-Order Filtering:** The 7th-tuned LC branch presents a significantly lower impedance path for higher-order harmonic currents (such as the 11th and 13th components) than a branch tuned to the 5th harmonic.

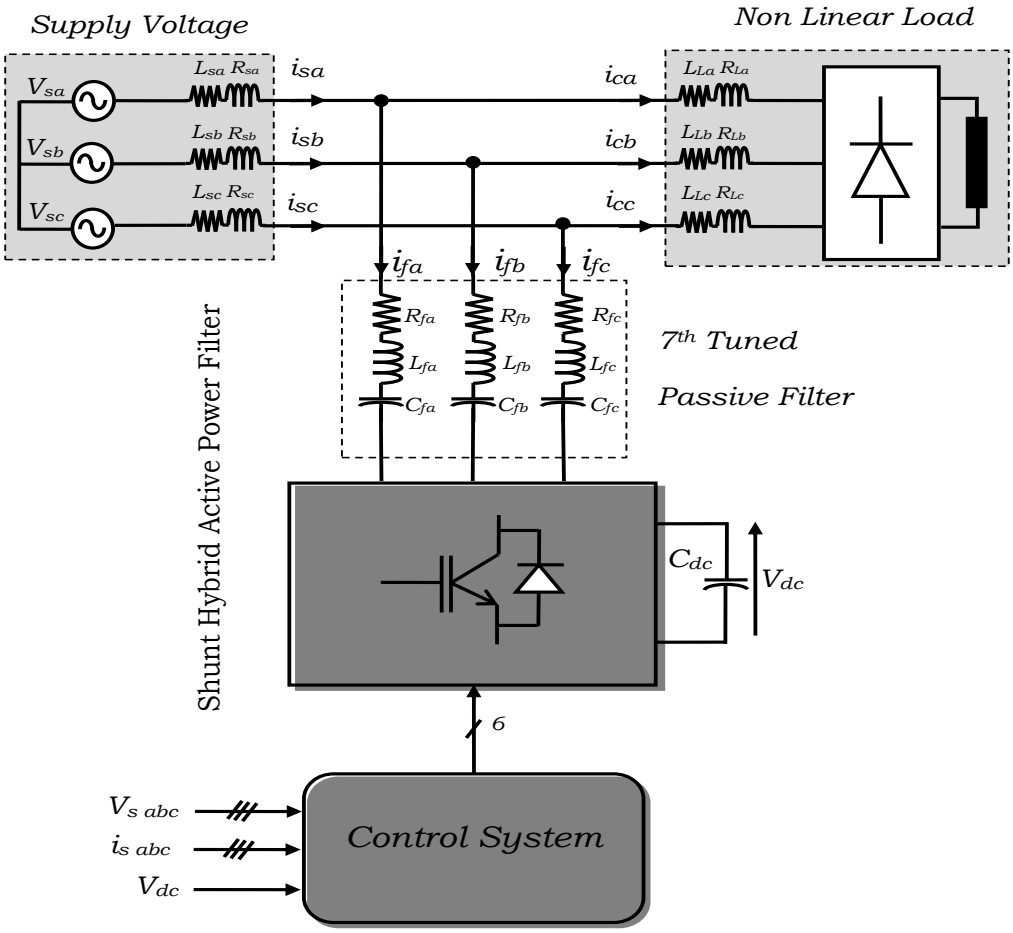

Figure1. Topology of the proposed SHAPF

The active power filter consists of a three-phase Pulse-Width Modulated (PWM) Voltage Source Inverter (VSI) using six Insulated Gate Bipolar Transistors (IGBTs) and a DC-link energy storage capacitor C_{dc}. This hybrid arrangement provides a substantial reduction in the inverter power rating and allows operation at a very low DC-bus voltage, as no fundamental grid line voltage is directly applied across the active inverter terminals—the grid voltage is predominantly supported by the passive filter capacitor.

2.1 Mathematical Principle of Harmonic Compensation

The single-phase equivalent circuit of Figure 1 is shown in Figure 2(a), where Z_s denotes the source impedance and Z_F represents the total impedance of the passive filter. The

active filter is modeled as a voltage source V_{AF} , and the load is represented by an ideal current source I_L.

Assuming a balanced, sinusoidal supply voltage, the source harmonic current I_{Sh} when no active filter is connected ($V_{AF} = 0$) is given by:

$$I_{Sh} = \frac{Z_F}{S.L_S + Z_F} I_{Lh} \quad (1)$$

If the supply impedance $\omega h L_s$ is significantly smaller than Z_F, the desired filtering characteristics cannot be achieved. Furthermore, harmonic resonance between L_s and Z_F may occur at a specific frequency, resulting in the harmonic-amplification phenomenon. When the active filter is connected, it assists the passive filter in absorbing the load harmonic current I_{Lh}, thereby minimizing the harmonic current flowing into the supply. Additionally, the active filter effectively damps out harmonic resonance. Under these conditions, the supply harmonic current I_{Sh}, the terminal harmonic voltage V_{Th}, and the active filter output voltage V_{AF} are expressed as follows:

$$I_{Sh} = \frac{Z_F}{R + S.L_S + Z_F} I_{Lh} \quad (2)$$

$$V_{Th} = -\frac{S.L_S Z_F}{R + S.L_S + Z_F} I_{Lh} \quad (3)$$

$$V_{AF} = \frac{Z_F}{R + S.L_S + Z_F} I_{Lh} \quad (4)$$

Equation (2) shows that Figure 2(a) is equivalent to Figure 2(b) with respect to I_{Sh}. This implies that a pure resistor K (Ω) is connected in series with L_s, as illustrated in Figure 2(b).

If $K \gg Z_F$, all harmonic currents injected by the load sink into the LC filter. Conversely, if $K \ll \omega_h L_S$, K dominates the filtering characteristics. Furthermore, K acts as a damping resistor to eliminate parallel harmonic resonance between L_S and Z_F. In short, the underlying principle is to simultaneously increase Z_S and decrease Z_F [8–10].

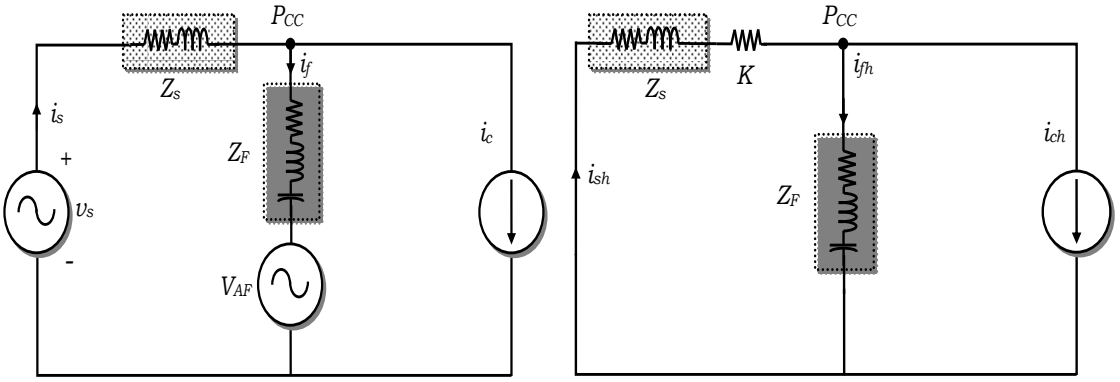

Figure 2. Single Phase equivalent circuit

Figure 3 illustrates the filtering characteristics (the relationship between I_{Sh} and I_{Lh}) of the hybrid filter for various values of K.

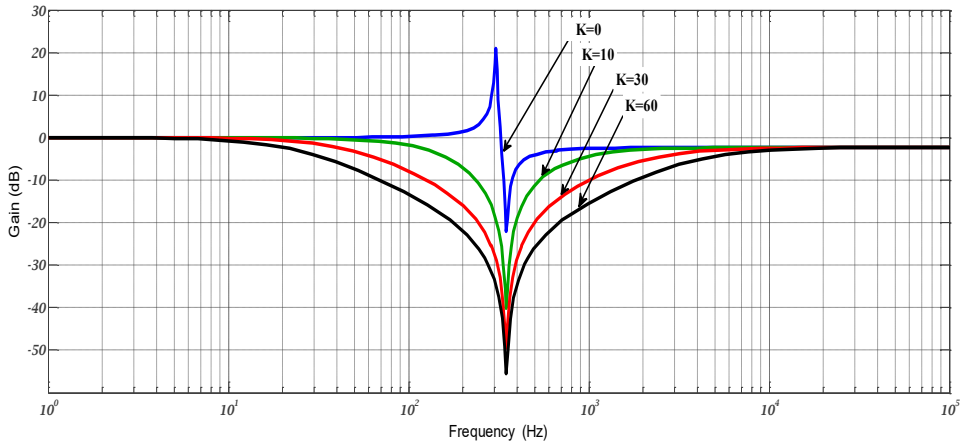

Figure 3. Filtering characteristics

When the active filter is not connected in series with the LC filter, a harmonic-amplification phenomenon occurs within the 200–700 Hz frequency range. Conversely,

when the active filter is incorporated, this harmonic amplification is entirely eliminated. However, the filtering performance of the hybrid filter remains satisfactory only at the seventh harmonic frequency.

3. **Advanced Control Strategy of the Proposed SHAPF**

The operational diagram of the proposed SHAPF control strategy is depicted in Figure 4. This system samples the DC-bus voltage (V_{dc}), alongside the three-phase grid currents (I_{sabc}) and voltages (V_{sabc}), to generate the pulse-width modulation (PWM) reference voltages (V^*_{sabc}) for the voltage source inverter. Operationally, the measured line currents (I_{sa}, I_{sb}, and I_{sc}) are converted into d-q axis active (I_d) and reactive (I_q) components via a synchronous reference frame (SRF). This reference frame rotates at the fundamental frequency and is synchronized with the positive-sequence component of the grid voltage [5].

$$\begin{bmatrix} i_d \\ i_q \end{bmatrix} = \frac{2}{3} \begin{bmatrix} \cos\hat{\theta} & \cos\left(\hat{\theta} - \frac{2\pi}{3}\right) & \cos\left(\hat{\theta} + \frac{2\pi}{3}\right) \\ -\sin\hat{\theta} & -\sin\left(\hat{\theta} - \frac{2\pi}{3}\right) & -\sin\left(\hat{\theta} + \frac{2\pi}{3}\right) \end{bmatrix} \begin{bmatrix} i_{S_a} \\ i_{S_b} \\ i_{S_c} \end{bmatrix} \tag{5}$$

In this formulation, $\hat{\theta}$ denotes the phase angle of the system voltage's positive-sequence component, which is extracted using the robust phase-locked loop (PLL) introduced in this work. Given that the target topology is a three-phase three-wire system, the zero-sequence component is omitted, leaving only the d-axis (I_d) and q-axis (I_q) current variables under analysis. Furthermore, both the active and reactive current channels can be split into their respective DC (fundamental) and AC (harmonic) parts.

$$\begin{bmatrix} i_d \\ i_q \end{bmatrix} = \begin{bmatrix} i_{d_{DC}} + i_{d_{AC}} \\ i_{q_{DC}} + i_{q_{DC}} \end{bmatrix} \tag{6}$$

In this expression, $\bar{\imath}_d$ and $\bar{\imath}_q$ denote the continuous (DC) d-axis and q-axis components, which represent the fundamental active and reactive currents, respectively. Conversely, $\tilde{\imath}_d$ and $\tilde{\imath}_q$ signify the alternating (AC) components, corresponding to the harmonic active and reactive current demands.

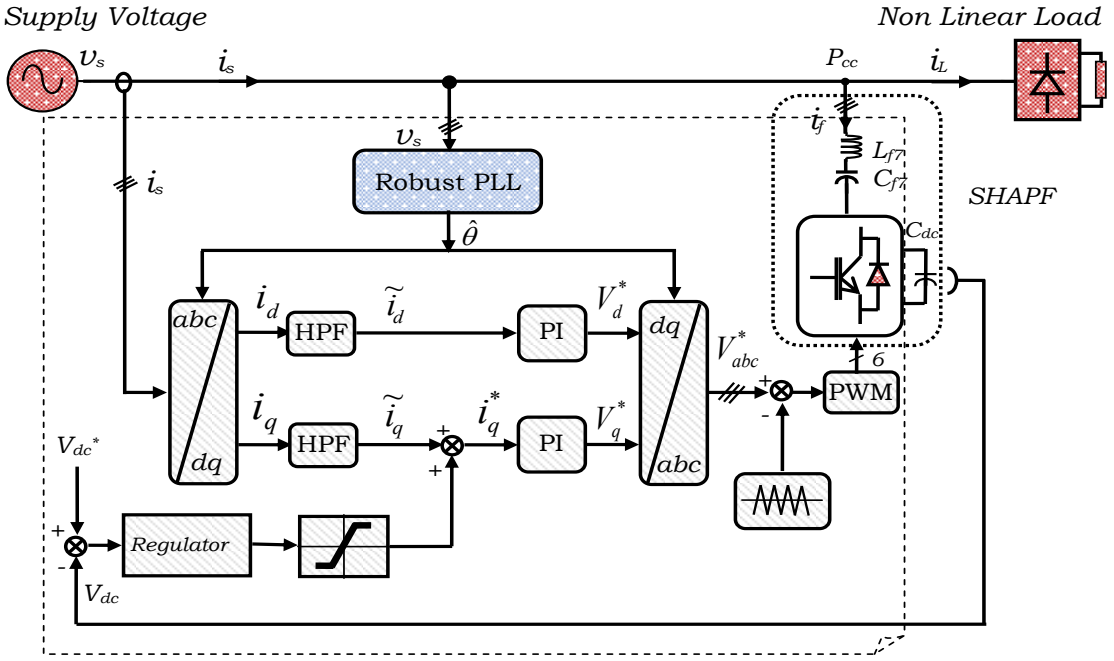

Figure 4. The SHAPF Control diagram

The control objective is for the utility grid to furnish exclusively the DC portion of the active current, while the SHAPF compensates for its AC harmonic components along with the total reactive current. Regarding reactive power demand, the passive filter absorbs its fundamental (DC) component, whereas the inverter delivers an AC voltage to attenuate harmonic resonance.

To isolate the AC components ($\tilde{\imath}_d$) from i_d, a second-order low-pass filter (LPF) with a 12 Hz cutoff frequency is employed. The resulting harmonic current reference $\tilde{\imath}_d$, together with i_q^*, is processed through proportional-integral (PI) controllers to synthesize the

inverter's voltage reference signals. Subsequently, an inverse synchronous frame transformation ($dq \rightarrow abc$) converts these voltage commands back into three-phase quantities. Finally, sinusoidal pulse-width modulation (SPWM) yields the switching signals required to execute harmonic isolation and preserve DC-bus voltage balance.

3.1 DC-Bus Voltage Regulation and Anti-Windup Control

The active filter is capable of establishing and maintaining the DC-capacitor voltage autonomously, eliminating the need for an external auxiliary power source. The DC-bus voltage control scheme, which incorporates a proportional-integral (PI) regulator, is depicted in Figure 5. By controlling the active filter to generate a fundamental voltage component synchronized in phase with the leading fundamental current of the passive filter, active power flows into the DC capacitor. As a result, the control variable managed within the DC-bus voltage feedback loop is ΔI_q rather than ΔI_d [8].

Given a high switching frequency, the inner current loop operates with a significantly higher bandwidth than the outer DC voltage loop. Under this dynamic decoupling condition, the poles of the inner loop transfer function do not affect the stability of the outer control loop. Consequently, the steady-state closed-loop current gain can be approximated as unity ($I_s(s)/I_s^*(s) = 1$), allowing the overall control structure in Figure 5(a) to be simplified. The parameters of the PI controller (K_p, K_i) are subsequently selected based on the step-response characteristics of this reduced-order model. Additionally, an anti-windup mechanism is integrated into the PI voltage regulator (Figure 5(b)) to suppress current spikes and smooth transients during startup and load perturbations. The mathematical model of the voltage control loop is expressed as:

$$\frac{V_{dc}^{*}}{V_{dc}} = \frac{\frac{K_p}{C_{dc}}.S + \frac{K_i}{C_{dc}}}{S^2 + \frac{K_p}{C_{dc}}.S + \frac{K_i}{C_{dc}}} \tag{7}$$

Based on (7), the closed-loop transfer function relating the actual DC-bus voltage (V_{dc}) to its reference value (V_{dc}^{*}) can be modeled as a second-order system of the form:

$$\frac{V_{dc}^{*}}{V_{dc}} = \frac{2.\xi\omega_n.S + \omega_n^{2}}{S^2 + 2.\xi\omega_n.S + \omega_n^{2}} \tag{8}$$

where ω_n represents the natural frequency and ξ denotes the damping ratio. The presence of two poles and a zero in this transfer function demonstrates that the proposed anti-windup PI voltage controller guarantees rapid dynamic response alongside robust stability during transient conditions.

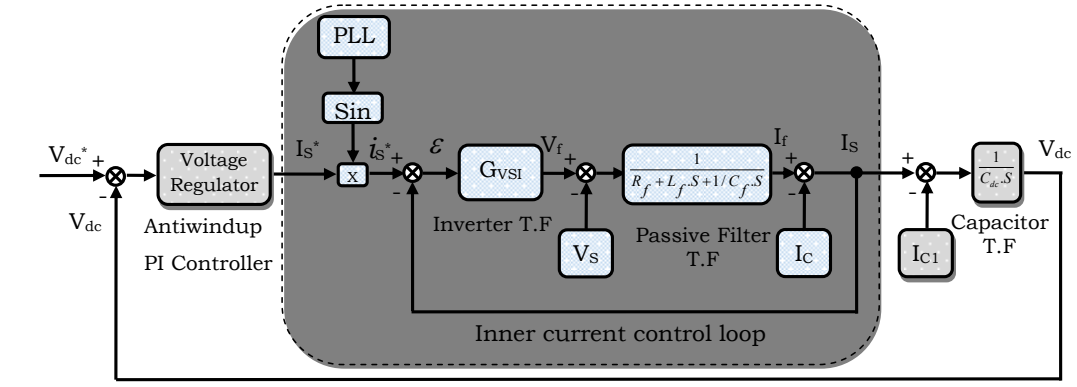

(a)

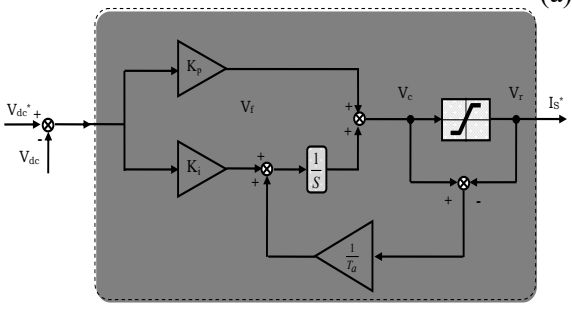

(b)

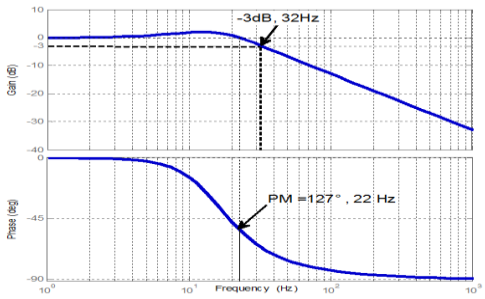

(c)

Figure 5. Bloc diagram of the DC-bus voltage control

By equating the coefficients of (5) and (6), the PI parameters K_p and K_i are derived as follows [14,15]:

$$K_p = 2\xi\omega_n C_{dc}$$

$$K_i = C_{dc}\omega_n^2$$

Furthermore, the frequency-domain analysis presented in the Bode plot of Figure 5(c) confirms strong system stability, exhibiting a phase margin (PM) of $127°$ and a bandwidth (BW) of 62 rad/s.

3.2 Robust MVF-Based Phase-Locked Loop (PLL) Design

The primary objective of the control strategy presented in this paper is to enhance the performance of the SHAPF by integrating a robust phase-locked loop (PLL). Powered by a Multi-Variable Filter (MVF), this advanced PLL directly extracts the fundamental voltage components along the α--β axes. As a result, it renders the synchronization process highly resilient to grid disturbances, particularly harmonic distortion and voltage unbalance [16,17].

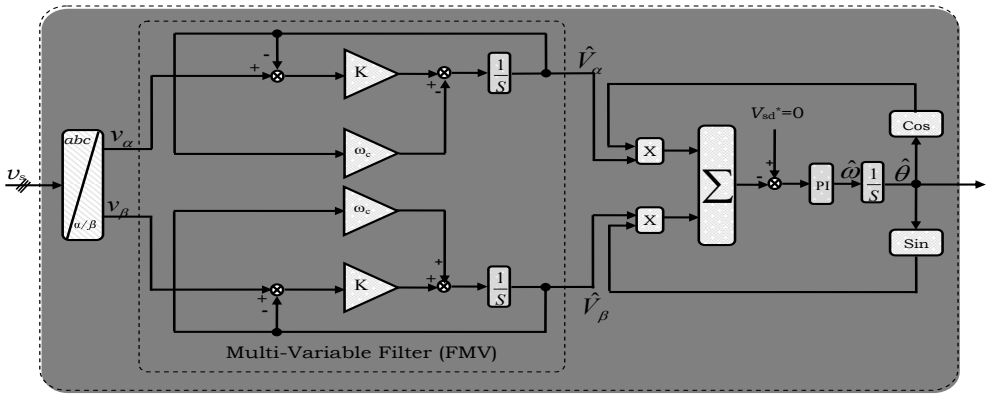

Figure 6. Robust PLL principle scheme

The overall structure of the proposed robust PLL is depicted in Figure 6. The core component of this scheme is the MVF defined in (7), which isolates the fundamental stationary frame (α--β) voltage signals at the grid frequency (50 Hz). Crucially, this filtering process achieves unity gain ($|H(s)| =$ 0 dB) at 50 Hz without introducing any phase displacement or amplitude distortion (Figure 7). In this formulation, ω_c and k represent the cutoff frequency and dynamic gain of the filter, respectively.

$$\hat{V}_\alpha(s) = \frac{k(s+k)}{(s+k)^2+\omega_c{}^2}.V_\alpha(s) - \frac{k.\omega_c}{(s+k)^2+\omega_c{}^2}.V_\beta(s)$$
$$\hat{V}_\beta(s) = \frac{k(s+k)}{(s+k)^2+\omega_c{}^2}.V_\beta(s) + \frac{k.\omega_c}{(s+k)^2+\omega_c{}^2}.V_\alpha(s) \quad (7)$$

The three-dimensional Bode diagram of the Multi-Variable Filter yields the frequency response characteristics illustrated in the following figure:

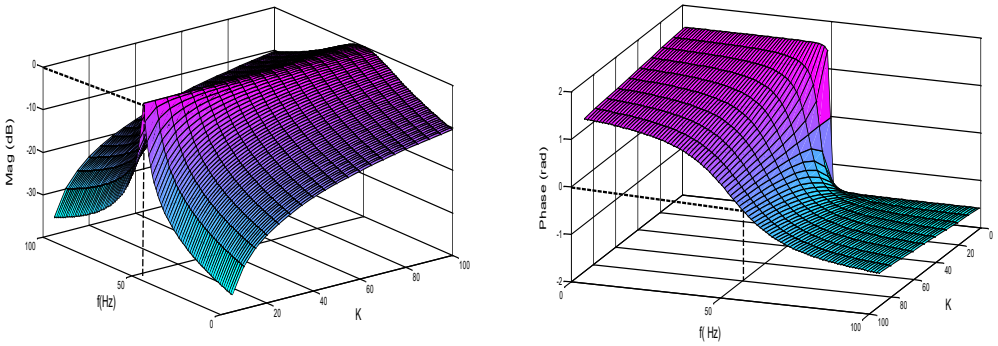

(a) (b)

Figure 7. Bode diagram of Multi-Variable Filter a) magnitude and b) phase versus f and K

As indicated in Figure 7, the phase response of the Bode diagram drops to zero at 50 Hz, confirming that the output signals remain perfectly in phase with the inputs. To validate performance under severe operating conditions, Figure 8 presents the simulation results of the robust PLL during extreme grid disturbances. Specifically, Figure 8(a) displays a highly polluted supply voltage contaminated with severe harmonic distortion and random noise. In contrast, Figure 8(d) demonstrates the balanced, purely sinusoidal voltage signals extracted by the proposed robust PLL. These findings confirm the filter's exceptional capability to attenuate grid voltage harmonics without introducing phase lag, while effectively eliminating unbalance across the electrical network.

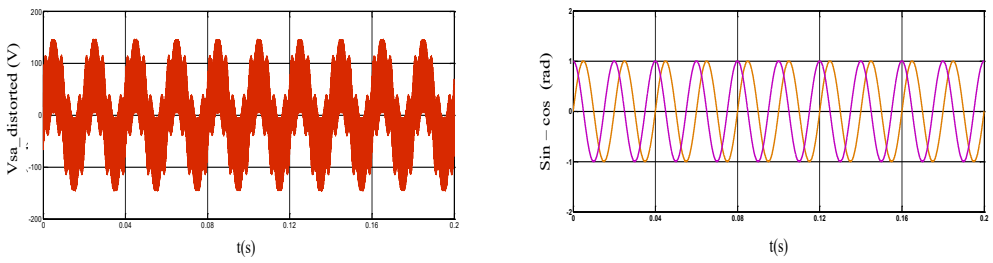

(a) (b)

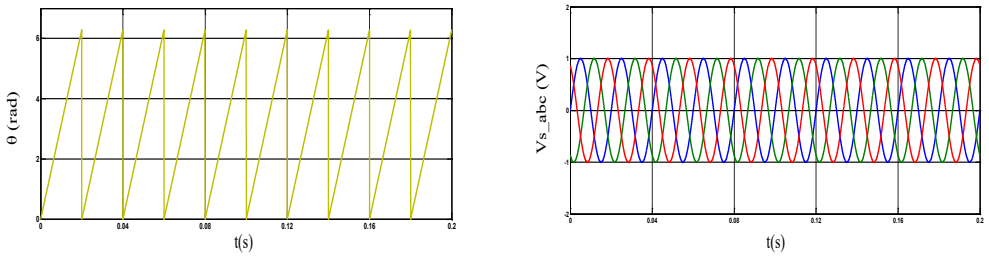

(c) (d)

Figure 8. Robust PLL simulation results

4. Simulation Setup and Performance Analysis

To evaluate the performance of the proposed SHAPF control strategy, a simulation model was implemented in the MATLAB/Simulink environment using the SimPower Systems blockset.

Table 1. System components and parameters values

Supply Voltage	V_{Sabc} = 50V (rms)	Quality Factor Q	42
Line frequency	f =50 Hz	APF DC-capacitor	C_{dc} = 1100 µF
Supply line impedance	R_S=0.1 Ω , L_S =0.05 mH	APF DC-bus voltage	V_{dc}^* = 15 V
Nonlinear load components	R_L=0.1 Ω , L_L=0.05 mH R_{D1}=16.1 Ω , R_{D2} =30 Ω L_D =1 mH	Voltage regulator Parameters	K_{pv}=0.156, K_{iv}=11.1
		Current regulator Parameters	K_{pc}=0.156, K_{ic}=11.1
		Resonant frequency	350 Hz
7^{th} tuned passive filter	L_{F7} =1.9 mH, L_{C7} =110µF	LPF Cut-off frequency	f_{LPF} = 12 Hz

The overall active filter architecture consists of four main components: a three-phase power supply, a non-linear load comprising a three-phase diode bridge rectifier feeding an inductive load, a pulse-width modulation (PWM) voltage source inverter, and the main control block. To maintain consistency, the simulation parameters match the experimental setup and are summarized in Table 1.

Numerical simulations were conducted to evaluate the viability and filtering performance of the proposed hybrid system. Figure 9 illustrates the initial system behavior prior to

connecting the filter under a polluted grid environment caused by the non-linear load. As shown in Figure 9(d), the absence of both active and passive filtering leads to severe harmonic pollution, with the supply current (I_s) exhibiting a high total harmonic distortion ($THD_i = 27.38\%$). Harmonic spectrum analysis reveals that the non-linear load predominantly generates 5th, 7th, 9th, and 11th order harmonic currents, with the 5th harmonic component displaying the highest amplitude.

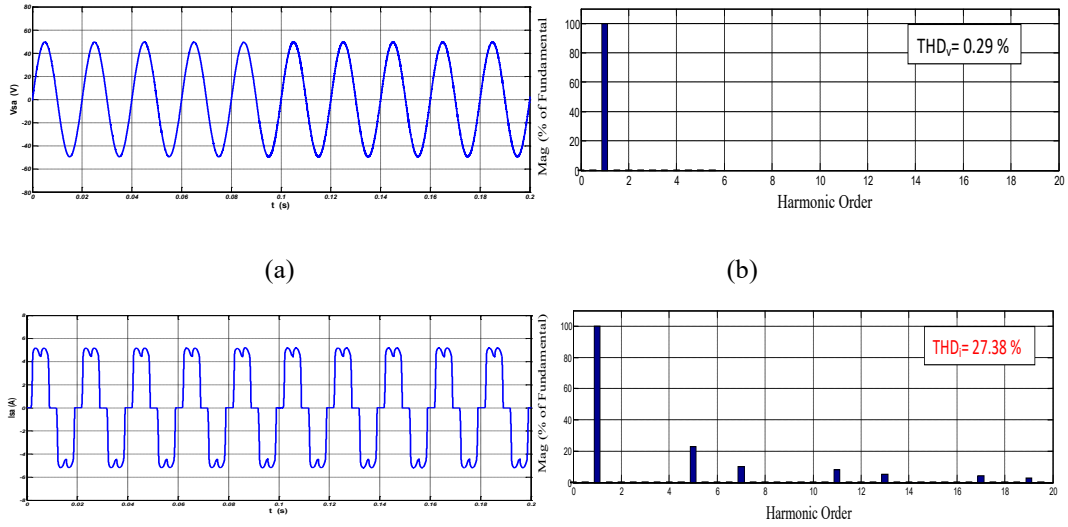

Figure 9. Simulation waveforms before connecting the SHAPF

The subsequent section evaluates the system's performance through numerical simulations under both steady-state and transient operating conditions.

Figures 10 illustrates the time-domain waveforms of the supply voltage (V_{sa}), load current (I_{ca}), supply current (I_{sa}), DC-bus voltage (V_{dc}), active power (P), and reactive power (Q). Prior to activating the SHAPF, the grid current is heavily distorted; however, upon connecting the active filter at $t = 0.08$ s, the supply current total harmonic distortion (THD_i) drops drastically from 27.38% to 2.71%. The resulting current waveform becomes near-sinusoidal, demonstrating the high efficacy of the proposed SHAPF control strategy in suppressing harmonic distortion.

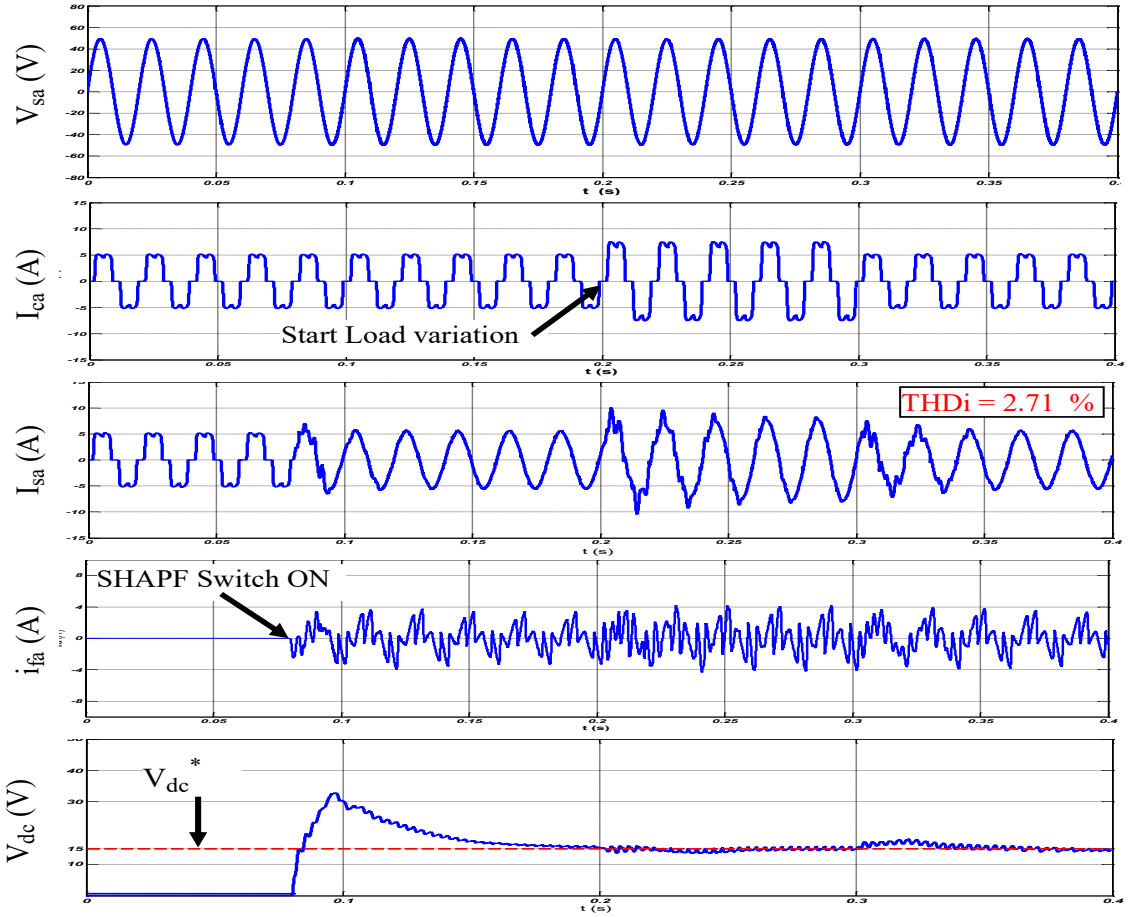

Figure 10. Simulation waveforms after connecting the SHAPF in transient state

To assess dynamic resilience, step-change load perturbations were applied to the non-linear load's DC side—transitioning from R_{D2} to R_{D1} at $t = 0.2$ s, and reverting from R_{D1} to R_{D2} at $t = 0.3$ s. Following these load step variations, the supply current experiences a minor transient distortion lasting approximately one line cycle ($\sim$ 20 ms). This rapid recovery duration guarantees that adjacent sensitive equipment and external circuits remain unaffected. Furthermore, the DC-bus voltage (V_{dc}) remains tightly regulated throughout these transient intervals, validating the anti-windup PI controller's ability to prevent windup phenomena and maintain rapid DC-link stabilization.

5. **Experimental Validation**

The real-time performance of the proposed SHAPF was experimentally validated using

the laboratory test bench developed at the LIAS-ENSIP Laboratory, University of Poitiers (Figure 12). The system is interfaced to the grid via a 20 kVA, 400/230 V step-down transformer. The active power filter topology employs a 20 kVA three-phase voltage source inverter (VSI) equipped with 1200 V, 50 A IGBT modules (SKM 50 GB 123D). Signal isolation and dead-time management for the gate control signals are handled by a custom driver board based on IXDP630 integrated circuits alongside SEMIKRON SKHI 22 gate drivers.

The control algorithm was executed in real time using a dSPACE DS1104 controller board configured within the MATLAB/Simulink Real-Time Workshop (RTW) environment, running at a sampling period (T_s) of 50 μs [17–19].

Figure 12. Photography of the APF system prototype

Figures 13(a) and 13(b) depict the experimental performance of the robust PLL when subjected to heavily polluted and unbalanced grid voltages. In contrast, Figures 13(c) and 13(d) present the synchronized, balanced sinusoidal signals synthesized by the proposed PLL scheme. Consistent with the simulation findings, these experimental results verify the PLL's capability to isolate fundamental components from harmonic-polluted and asymmetrical grid conditions without introducing phase displacement [19].

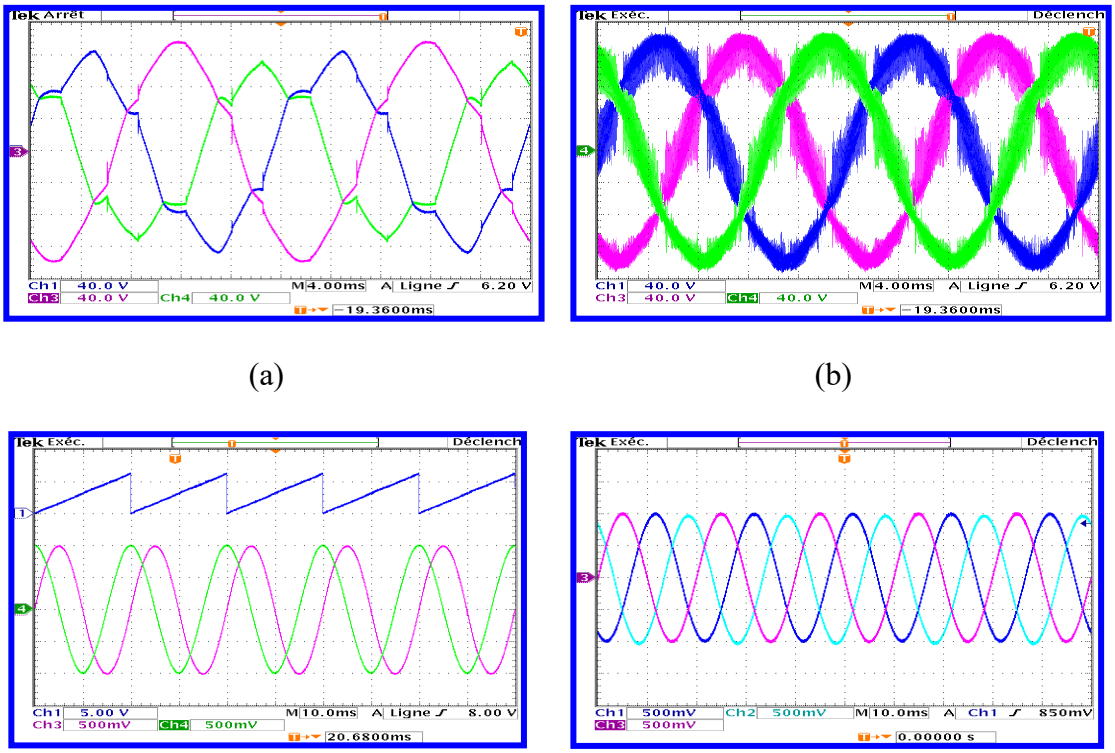

(a) (b)

(c) (d)

Figure13. Robust PLL experimental results

Figure 14 presents the experimental measurements obtained prior to connecting the filter to the polluted grid. In the uncompensated state (without passive or active filtering), the supply current exhibits severe harmonic distortion, reaching a total harmonic distortion (THD_i) of 23% due to the non-linear load. Spectrum analysis confirms that the non-linear load predominantly draws 5th, 7th, 9th, and 11th order harmonic components, with the 5th harmonic exhibiting the dominant magnitude. These experimental observations show strong agreement with the preliminary simulation results.

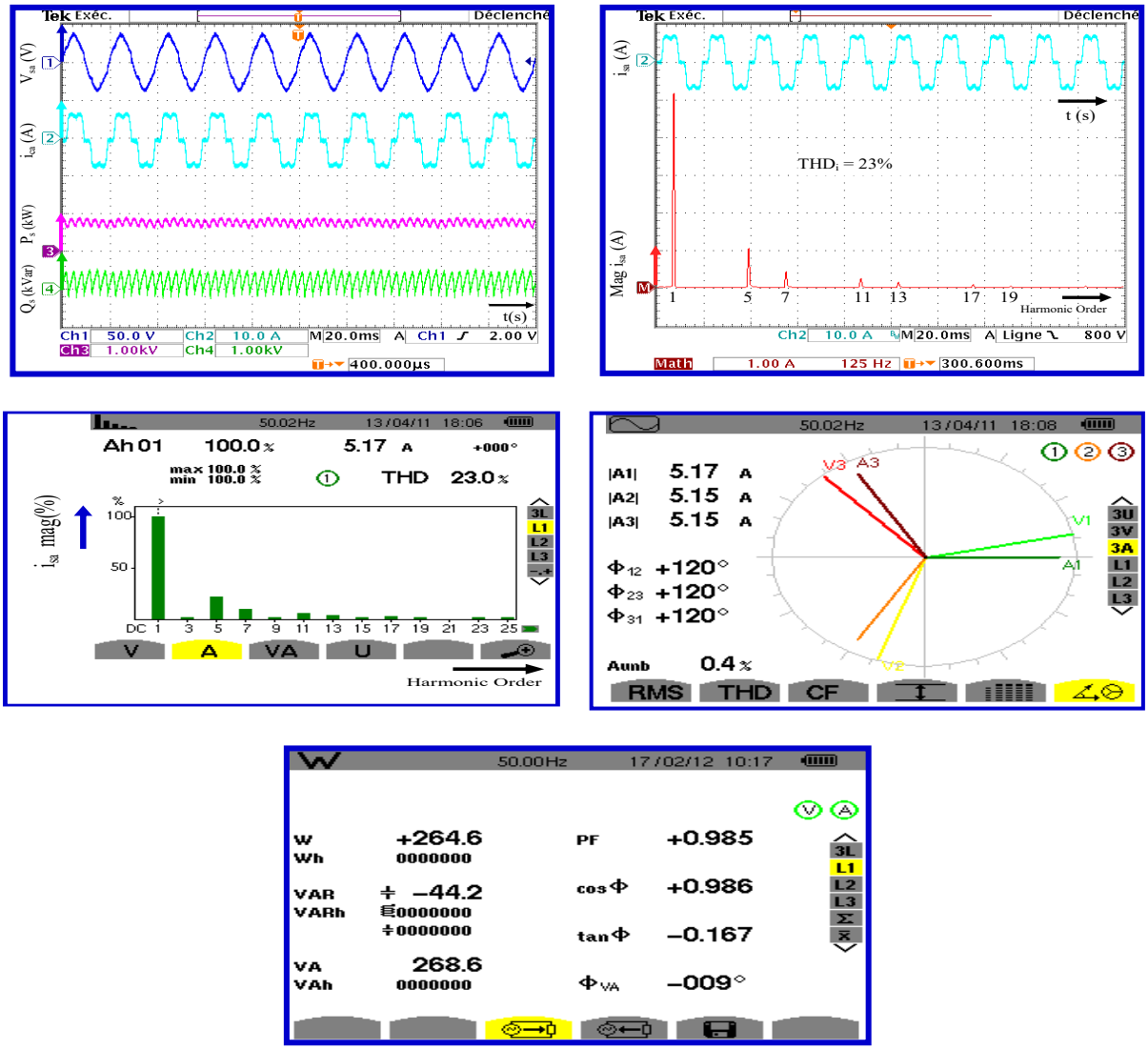

Figure 14. Experimental waveform before connection of the SHAPF

The steady-state experimental performance of the system is summarized in Figure 15. Figures 15(a) and 15(b) depict the time-domain waveforms for the supply voltage (V_{sa}), load current (I_{ca}), compensated supply current (I_{sa}), active power (P), reactive power (Q), and the DC-bus voltage (V_{dc}), which remains tightly regulated at its target setpoint of 15 V.

Upon activating the SHAPF, the supply current total harmonic distortion (THD_i) drops significantly from an initial 23% (or 27.38% under uncompensated baseline conditions) down to 3.9% (compared to 2.7% obtained in simulations), as illustrated in Figures 16(a)

and 16(b).

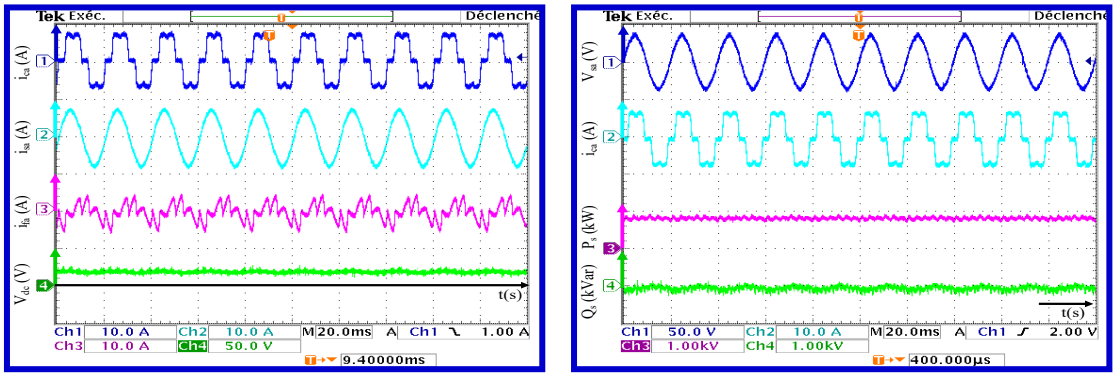

(a) (b)

Figure 15. Experimental waveform after connection of the SHAPF

The resulting grid current transitions to an almost purely sinusoidal profile, confirming the practical efficacy of the proposed SHAPF control strategy in real-time harmonic mitigation. Additionally, the DC-bus voltage (V_{dc}) exhibits exceptional dynamic stability across operating conditions, validating the anti-windup PI controller's capability to suppress windup effects and maintain steady DC-link voltage regulation.

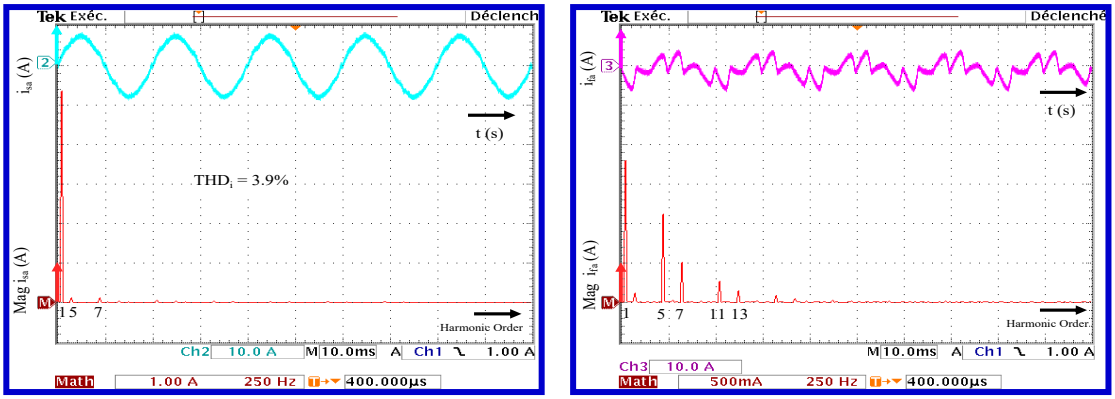

(a) (b)

Figure 16. Supply and compensating currents with their spectrums

6. **Conclusion**

This paper presented a Shunt Hybrid Active Power Filter (SHAPF) designed to enhance grid power quality and compensate for reactive power demands induced by non-linear

loads. The proposed control framework operates in the synchronous reference frame (SRF) at fundamental frequency, integrating a Multi-Variable Filter (MVF) alongside a robust PLL to achieve precise signal isolation under adverse grid conditions.

The physical system topology combines a single 7th-harmonic tuned LC passive filter per phase directly in series with a low-rated three-phase active power filter, entirely omitting the need for an intermediate coupling transformer. Consequently, the power rating requirement of the active filter is significantly reduced compared to standard standalone active power filters.

The advanced control architecture ensures high harmonic attenuation capabilities alongside fast dynamic response. Extensive numerical simulations and experimental validations conducted under both steady-state and transient operating regimes confirm the robustness, practical viability, and overall efficacy of the proposed transformerless SHAPF system.

References

[1] Akagi H. New trends in active filters for power conditioning. IEEE Trans. Ind. App.1996; 32: 1312–1322.

[2] G. Boudechiche, M. Sarra, O. Aissa, and J. P. Gaubert, "Solar SAPF based on DPC with disturbance rejection principle: study and simulation," Journal of Engineering Research, 2021, doi: 10.36909/jer.v9i

[3] G. Boudechiche, M. Sarra, O. Aissa, and J. P. Gaubert, "An investigation of solar active power filter based on direct power control for voltage quality and energy transfer in grid-tied photovoltaic system under unbalanced and distorted conditions," Journal of Engineering Research, vol. 9, no. 3B, pp. 168–188, 2021, doi: 10.36909/jer.v9i3B.9061.

[4] H. Fujita and H. Akagi, "A practical approach to harmonic compensation in power systems—series connection of passive and active filters," IEEE Transactions on Industry Applications, vol. 27, no. 6, pp. 1020–1025, Nov./Dec. 1991, doi: 10.1109/28.108451.

[5] H. Fujita and H. Akagi, "An approach to harmonic-free AC/DC power conversion for large industrial loads: the integration of a series active filter with a double-series diode rectifier," IEEE Transactions on Industry Applications, vol. 33, no. 5, pp. 1233–1240, Sep./Oct. 1997, doi: 10.1109/28.633802.

[6] S. Bhattacharya, P.-T. Cheng, and D. M. Divan, "Hybrid solutions for improving passive filter performance in high power applications," IEEE Transactions on Industry Applications, vol. 33, no. 3, pp. 732–747, May/Jun. 1997, doi: 10.1109/28.585864.

[7] H. Akagi, A. Nabae, and S. Atoh, "Control strategy of active power filters using multiple voltage-source PWM converters," IEEE Transactions on Industry Applications, vol. IA-22, no. 3, pp. 460–465, May/Jun. 1986, doi: 10.1109/TIA.1986.4504743.

[8] W. Tangtheerajaroonwong, T. Hatada, K. Wada, and H. Akagi, "Design and performance of a transformerless shunt hybrid filter integrated into a three-phase diode rectifier," IEEE Transactions on Power Electronics, vol. 22, no. 5, pp. 1882–1889, Sep. 2007, doi: 10.1109/TPEL.2007.904207.

[9] S. Srianthumrong and H. Akagi, "A medium-voltage transformerless AC/DC power conversion system consisting of a diode rectifier and a shunt hybrid filter," IEEE Transactions on Industry Applications, vol. 39, no. 3, pp. 874–882, May/Jun. 2003, doi: 10.1109/TIA.2003.810660.

[10] S. Srianthumrong, H. Fujita, and H. Akagi, "Stability analysis of a series active filter integrated with a double-series diode rectifier," IEEE Transactions on Power Electronics, vol. 17, no. 1, pp. 117–124, Jan. 2002, doi: 10.1109/63.988838.

[11] B.-R. Lin, B.-R. Yang, and H.-R. Tsai, "Analysis and operation of hybrid active filter for harmonic elimination," Electric Power Systems Research, vol. 62, no. 3, pp. 191–200, Jul. 2002, doi: 10.1016/S0378-7796(02)00072-0.

[12] S. G. Dan, R. Magureanu, L. Asiminoaei, R. Teodorescu, and F. Blaabjerg, "DSP control of line hybrid active filter," in Proceedings of the IEEE International Symposium on Industrial Electronics (ISIE), Dubrovnik, Croatia, Jun. 2005, vol. 4, pp. 1729–1734, doi: 10.1109/ISIE.2005.1529194.

[13] H. Na, W. Jian, and X. Dianguo, "A Novel Shunt Hybrid Power Filter for Suppressing Harmonics," in Proceedings of the IEEE International Symposium on Industrial Electronics (ISIE), Montreal, QC, Canada, Jul. 2006, vol. 2, pp. 1155–1160, doi: 10.1109/ISIE.2006.255389.

[14] M. Sarra, K. Djazia, A. Chaoui, and F. Krim, "Three-phase Active Power Filter with Proportional Integrator control," Journal of Electrical Systems, special issue 1, pp. 79–84, 2009, doi: 10.5281/zenodo.10091383.

[15] M. C. Benhabib and S. Saadate, "A new robust experimentally validated phase locked loop for power electronic control," EPE Journal, vol. 15, no. 3, pp. 36–48, Aug. 2005, doi: 10.1080/09398368.2005.11463595.

[16] M. Sarra, J. P. Gaubert, A. Chaoui, and F. Krim, "Experimental validation of two control techniques applied to a three phase shunt active power filter for power quality improvement," International Review of Electrical Engineering (IREE), vol. 6, no. 6, pp. 2825–2836, Nov. 2011 (ISSN: 1827-6660).

[17] M. Sarra, J. P. Gaubert, A. Chaoui, and F. Krim, "Control strategy of a transformerless three phase shunt hybrid power filter using a robust PLL," in Proceedings of the 38th Annual Conference of the IEEE Industrial Electronics Society (IECON 2012), Montreal, QC, Canada, Oct. 2012, pp. 1258–1267, doi: 10.1109/IECON.2012.6388557.